ACS OMEGA

http://pubs.acs.org/journal/acsodf

Article

Effect of Cross-Linking and Surface Treatment on the Functional Properties of Electrospun Polybenzimidazole Separators for Lithium Metal Batteries

Ji Hye Jung,[⊥] Vijayalekshmi Vijayakumar,[⊥] Anupriya K. Haridas, Jou-Hyeon Ahn, and Sang Yong Nam*

Cite This: ACS Omega 2022, 7, 47784−47795

Read Online

ACCESS | Metrics & More | Article Recommendations | Supporting Information

ABSTRACT: In this work, electrospun PBI separators with a highly porous structure and nanofiber diameter of about 90−150 nm are prepared using a multi-nozzle under controlled conditions for lithium metal batteries. Cross-linking with *α*, *α*-dibromo-p-xylene and surface treatment using 4-(chloromethyl) benzoic acid successfully improve the electrochemical as well as mechanical properties of the separators. The resulting separator is endowed with high thermal stability and excellent wettability (1080 to 1150%) with commercial liquid electrolyte than PE and PP (Celgard 2400) separators. Besides, attractive cycling stability and rate capability in $LiFePO_4$/Li cells are attained with the modified separators. Prominently, CROSSLINK PBI exhibits a stable Coulombic efficiency of more than 99% over 100 charge−discharge cycles at 0.5 C, which is superior to the value of cells using commercial PE and PP (Celgard 2400) separators. The half cells assembled using the CROSSLINK PBI separator can deliver a discharge capacity of 150.3 mAh g^{-1} at 0.2 C after 50 cycles corresponding to 88.4% of the theoretical value of $LiFePO_4$ (170 mAh g^{-1}). This work offers a worthwhile method to produce thermally stable separators with noteworthy electrochemical performances which opens new possibilities to improve the safe operation of batteries.

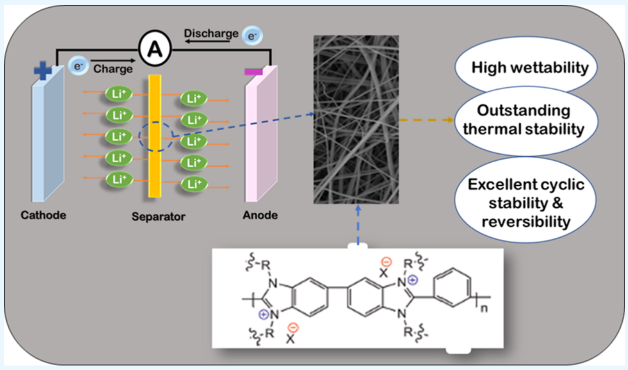

1. INTRODUCTION

Rechargeable lithium metal batteries with trustworthy electrochemical performances are considered to be the most promising energy storage devices in portable electronics, electric vehicles, as well as other energy storage devices.[1−4] A typical lithium metal battery is composed of five parts: electrodes (anode and cathode), current collectors, an electrolyte, a separator, and casing. As a key component of lithium metal batteries, a separator prevents direct contact between the electrodes to avoid internal short circuit while transmitting lithium ions in an efficient manner. Most critically, various characteristics of separators such as mechanical as well as thermal stability, porosity, electrolyte wettability, etc have a significant effect on the comprehensive performance of lithium metal batteries.[5,6] Currently, microporous membranes made of polyethylene (PE) and polypropylene (PP) are the most commercially used separators owing to their low cost, mechanical and chemical stabilities, electrochemical inertness, and shutdown behavior. However, the biggest shortcoming associated with these separators is their dimensional instability at elevated temperatures due to the inherently low melting point (PE:130 °C; PP:160 °C) which can create severe safety issues during battery operation.[7−10] Furthermore, poor electrolyte wettability associated with its low porosity as well as low surface energy also makes commercial PE or PP separators difficult to use in the next-generation lithium metal batteries.[11,12] These limitations reduce ionic conductivity and battery performance. Therefore, considerable efforts have been devoted to solving these problems.[13−17] As the brightest strategy, aromatic polymers are widely selected as separators to enhance the safe operation of batteries under harsh conditions. Among the various aromatic polymers, polybenzimidazole (PBI) is a high-temperature and highly durable engineering material. Most PBIs are not easily oxidized and have a decomposition temperature, above 600 °C.[18−20] Polar nitrogen atoms in its imidazole ring enhance electrolyte wettability, and the rigid backbone structure possesses inherent flame retardancy to the polymer.[21] For example, Liang's group had studied porous PBI prepared by blending followed by the phase inversion process and reported high conductivity, electrolyte wettability, and thermal stability.[22]

Received: August 25, 2022
Accepted: December 1, 2022
Published: December 14, 2022

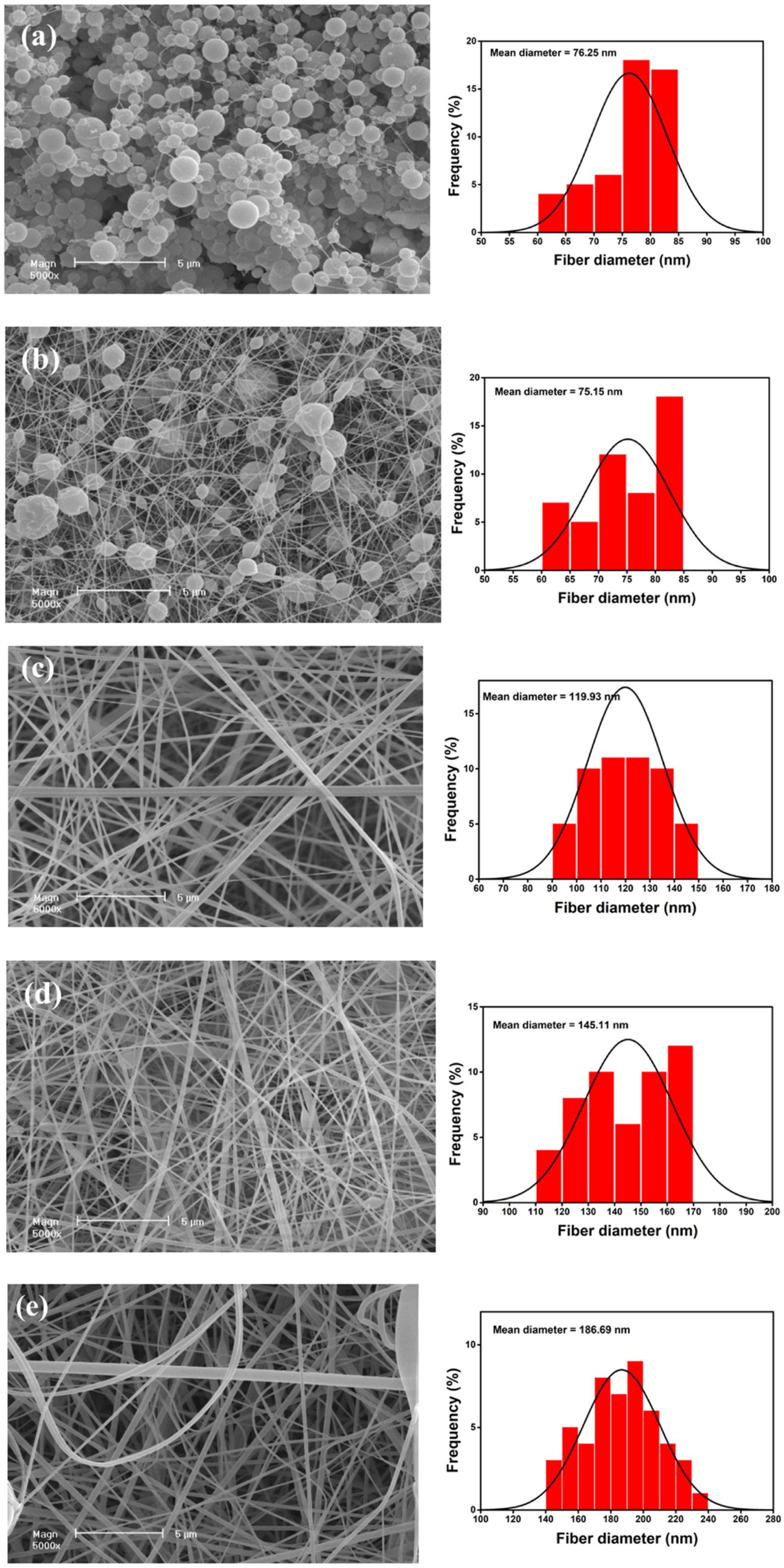

Figure 1. SEM images and nanofiber diameter distribution of various PBI membranes with different polymer concentrations: (a) 14 wt %, diameter of nanofiber: 60−85 nm, (b) 15 wt %, diameter: 62−85 nm, (c) 16 wt %, diameter: 90−150 nm, (d) 17 wt %, diameter: 110−170 nm, (e) 18 wt %, diameter: 140−240 nm.

Nowadays, electrospun nanofiber membranes owing to their interconnected and highly porous structure, high surface area, as well as excellent electrolyte absorption, have become a hot topic of research as high-performance battery separators. For example,

https://doi.org/10.1021/acsomega.2c05472
ACS Omega 2022, 7, 47784−47795

a poly(ether ether ketone) nanofibrous separator fabricated by Li et al. using the electrospinning technique demonstrated an electrolyte uptake of about 524% and an ionic conductivity of 3.81 mS cm^{-1}.[23] Lin et al. also made an electrospun poly(vinylidene fluoride) (PVDF) nanofibrous separator modified by poly(4-styrene sulfonic acid) lithium salt with superior electrochemical performance and durability in comparison to the commercial PP separators.[2] Lithium-ion battery separators fabricated from poly(vinylidene fluoride) (PVDF) and octyl phenyl polyhedral oligomeric silsesquioxane by electrospinning also exhibited good electrochemical performances and zero-dimensional shrinkage after heat treatment. The membrane exhibited an ionic conductivity of 4.2 mS cm^{-1}, an electrolyte uptake of 912%, and a mechanical strength of 12.7 MPa.[24] The electrospun polyimide (PI) and their copolymer-based composite separators possess high thermo-dimensional stability, porosity, as well as excellent electrochemical performance and ideal thermal shutdown function. Moreover, the polyimide separators are of benefit to the compatibility with electrolyte and reduce nucleation and plating overpotentials to form dendrite-like lithium deposit on the electrodes to enhance the cycle life.[25−27] Polyacrylonitrile (PAN) nanofiber membranes prepared by Dong et al. showed conductivity higher than that of commercial Celgard and a Coulomb efficiency as high as 98.7% after 50 cycles of battery performance at 0.5 C.[3] Even though the electrospun separators have an excellent porous structure, the low mechanical strength of various polymeric materials cannot meet the requirement of battery assembly and limits its application as battery separators.[28]

The purpose of this study is to develop a mechanically as well as thermally stable PBI separator with high porosity and electrolyte uptake through electrospinning followed by chemical treatment techniques. In this work, electrospinning using multi-nozzles was employed instead of a single nozzle which improves the consistency of fiber production, reducing spinning time and density of aggregation built up in one location.[29−31] Herein, electrospun PBI nanofibers are used as film-forming material and α, α'-dibromo-m-xylene (DBX) as the cross-linking agent. The cross-linked membranes were also treated with 4-(chloromethyl) benzoic acid (CMBA) to improve the electrolyte wettability. The effects of the DBX crosslinker and CMBA modifier on electrospun PBI separators prepared using multi-nozzles are yet to be reported to the best of our knowledge. The developed CROSSLINK PBI separator demonstrated excellent electrochemical performance and thermal stability in comparison to the commercial PE and PP (Celgard 2400) separators.

2. RESULTS AND DISCUSSION

2.1. Optimization of PBI Solution Concentration. The selection of the PBI solution concentration has a vital role in the spinning process and fabrication of the separators. The homogeneity has a pronounced impact on the successful performance of a separator and the composition as well as microstructure should be as uniform as possible throughout the material.[7] In this study, different PBI membranes using solutions of different concentrations (14, 15, 16, 17, and 18 wt %) were fabricated using the electrospinning process and their morphologies were observed using SEM analysis. Figure 1 shows the morphology and nanofiber diameter distribution of the prepared membranes. Fibrous structures with beads are formed at 14 and 15 wt % concentrations, and comparatively, more bead-like structures are observed at 14 wt %. On the other hand, all PBI concentrations of 16 wt % and more produced stable fibers, and the diameter of the fiber became larger with an increase in concentration and viscosity of the polymer solution. The formation of beads at low concentrations and increase in the diameter of fibers at high concentrations are related to the viscosity of the solution. The extent of polymer chain entanglement within the solution resulted in the variation of solution viscosity. Increase in the number of polymer molecules results in the increase in polymer chain entanglement and thereby viscosity. At low solution concentration and viscosity, the solution possesses a low viscoelastic force that is not capable of matching the electrostatic as well as Columbic repulsion force that stretch the electrospinning jet during the process, which results in a partial breakup of the jet. Furthermore, the greater number of free solvent molecules at low concentrations owing to the effect of surface tension comes together into a spherical shape, producing the formation of beads. Increase in polymer chain entanglement as well as improvement in viscoelastic force at high solution concentration prevents the breakup of jet and enables the solvent molecules to be distributed over the polymer molecules, leading to the smooth fiber formation with improved uniformity. The gradual increase in viscoelastic force with increase in solution concentration limits the stretching effect of the electrostatic as well as Columbic repulsion forces and increase the fiber diameter and its uniformity. The fine morphology and uniform nanofiber diameter distributions (90−150 nm) exhibited by PBI membranes at a concentration of 16 wt % realized their better fiber-forming performance. Therefore, the separators used in this study are fabricated with modified and pristine PBI solutions of 16 wt % concentration.

2.2. Morphology and Structure of Separators. Figure 2 shows the SEM images and photographs of the different

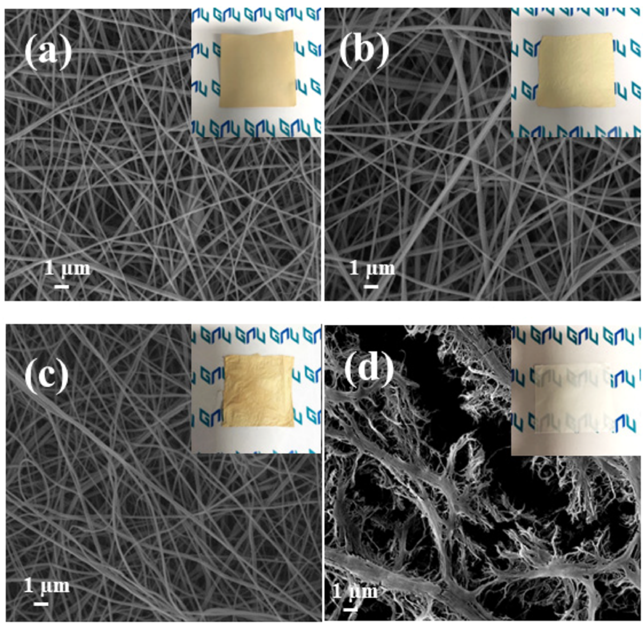

Figure 2. SEM images of surface of different separators: (a) PLAIN PBI, (b) CROSSLINK PBI, (c) CROSSLINK PBI−CMBA, and (d) Commercial PE.

separators. It is off-white and opaque across its surface. All PBI-based separators have a highly porous structure (see Table 1) than the commercial PE separator. In the case of the PLAIN PBI separator, the nanofibers formed are straight and smooth. However, after modification, the nanofiber structure became

https://doi.org/10.1021/acsomega.2c05472
ACS Omega 2022, 7, 47784−47795

Table 1. Porosity (*P*), Electrolyte Uptake (EU), and Mechanical Properties of the PBI Separator and Commercial PE Separator

property	PLAIN PBI	CROSSLINK PBI	CROSSLINK PBI-CMBA	commercial PE	Celgard 2400
P (%)	87 ± 3	70 ± 4	78 ± 3	40 ± 2	41 ± 3[40]
EU (%)	912 ± 4	1087 ± 4	1151 ± 3	439 ± 4	89.5 ± 3[40]
tensile strength (MPa)	3.61 ± 0.8	10.77 ± 1.2	8.91 ± 0.5	32.16 ± 1.2	128[44]
elongation at break (%)	36.11 ± 1.8	78.51 ± 2.2	53.17 ± 1.5	174.10 ± 2.5	76[44]
modulus (MPa)	22.25 ± 1.2	36.33 ± 2.4	23.74 ± 1.5	55.03 ± 2.5	348[44]

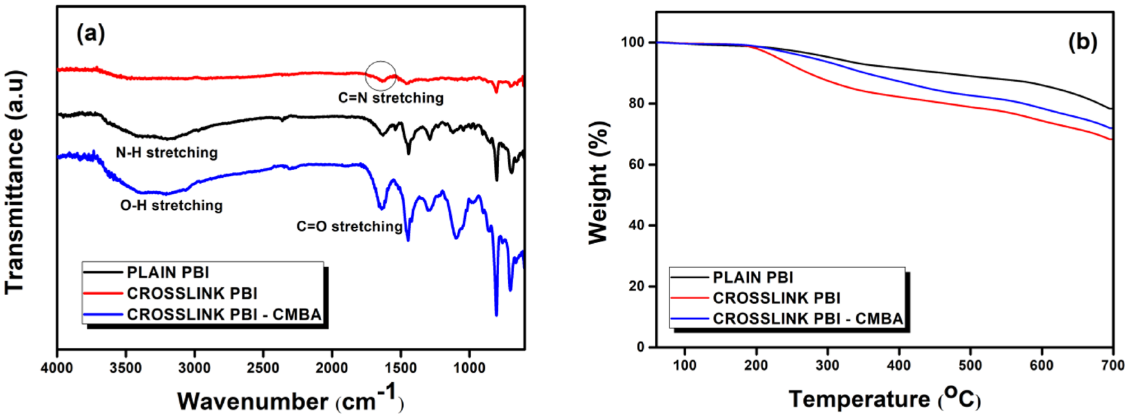

Figure 3. (a) FT-IR spectra and (b) TGA curves of electrospun PBI (PLAIN PBI), crosslinked electrospun PBI (CROSSLINK PBI), and cross-linked-CMBA-treated (CROSSLINK PBI-CMBA) electrospun PBI-based separators.

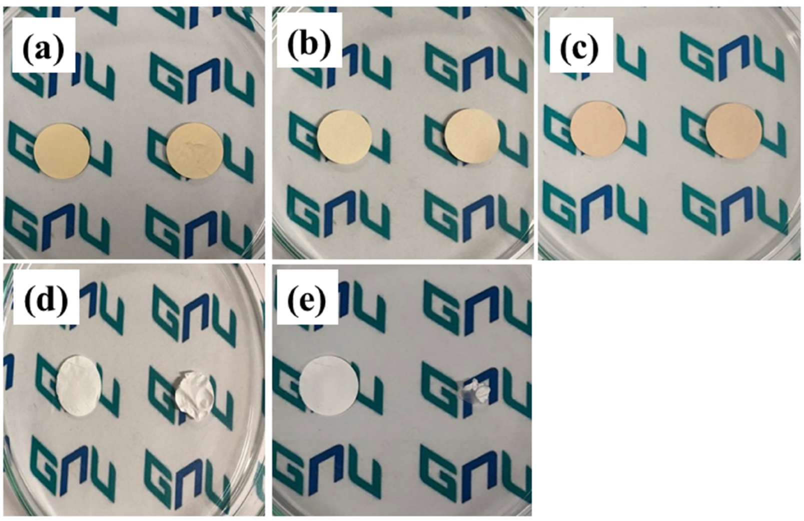

Figure 4. Thermal shrinkage (photographs before and after heat treatment) of (a) PLAIN PBI separator: 150 °C for 30 min, (b) CROSSLINK PBI at 150 °C for 30 min, (c) CROSSLINK PBI-CMBA at 150 °C for 30 min, (d) commercial PE separator at 120 °C for 10 min, and (e) commercial PE at 150 °C for 1 min.

slightly curvy and rough. This may be due to the contraction of the film during drying after being treated with α,α'-dibromo-m-xylene (DBX) and 4-(chloromethyl) benzoic acid (CMBA). The increase in roughness over time after being treated with sulfuric acid is also reported elsewhere.[32] With an increase in the exposure time and concentration of sulfuric acid, swelling and hence increase in fiber thickness and loosening were noticed in their work. The commercial PE separator possesses a porous microstructure with a thick tree-branch-like polymer phase, which may be dependent on the wet process conditions.[33] The cross-sectional morphology of PBI and the modified separator (Figure S1) also supported a typical nanofiber microstructure without any beads. The cryo-fractured cross-sectional morphology of CROSSLINK PBI exhibits a mechanically stable networked structure than that of PLAIN PBI. The pristine PBI and modified PBI separators in this work exhibit a random orientation of fibers that form a weblike interwoven network, and the gap between fibers may facilitate the film to possess better wettability and ion movement than the commercial PE separator.[23]

The chemical structure of the separators is confirmed by the FTIR spectra (Figure 3a). Typical PBI bands are noticed for the pristine PLAIN PBI membrane, including N−H stretching at 3600−3000 cm^{-1} and the C═N stretching vibration at 1613 cm^{-1}.[22] After cross-linking, the N−H and C═N peak intensities are decreased, indicating that these functional groups act as cross-linking sites in the reaction. The cross-linking mechanism is shown in Figure S2.[34] Moreover, after hydrophilization with

https://doi.org/10.1021/acsomega.2c05472
ACS Omega 2022, 7, 47784−47795

CMBA, the presence of the O−H band could be verified in the vicinity of 3600−3200 cm^{-1}, and the C═O band stretching is identified at around 1700 cm^{-1}, suggesting a successful modification of cross-linked PBI with CMBA.

2.3. Thermal Stability of Separators. The thermal stability of the separator is a property to guarantee safety especially for high-power batteries.[35] No significant weight loss is noticed up to 200 °C in the TGA thermogram of the separators (Figure 3b). The first weight loss observed between 200 and 450 °C is attributed to the loss of residual solvent and additives present in the system.[36,37] The main polymer starts to decompose as the temperature exceeds 450 °C because of its rigid molecular structure and high thermal stability and the weight retention of the separators is about 70 to 80% at 700 °C.[36] The CROSSLINK PBI separator shows more weight loss due to the degradation of cross-linking agent (α, α'-Dibromo-*m*-xylene, bp: 140 °C) and solvent (acrylonitrile, bp: 300 °C) present. Furthermore, the melting point of CMBA and sodium persulfate are at 201−202 °C and 180 °C in the CROSSLINK PBI-CMBA separator, respectively.[37] Commercial Celgard 2400 reported by Liang et al., however, showed comparatively lower main chain decomposition temperature (∼ 400 °C) and complete degradation as the temperature increased to 500 °C, indicating that PBI-based membranes have much better thermal stability than Celgard 2400.[22]

The thermal shrinkage of the separators was determined by measuring their dimensional change after storage at 150 °C for 30 min, and the photographs of the samples are shown in Figure 4. There is no significant change in the dimension and color observed in all the PBI-based separators expressed their outstanding thermal stability up to 150 °C, which is attributed to the superior thermal stability of imidazole groups and strong skeleton provided by PBI fibers. However, an apparent tendency in the reduction of dimensional stability with temperature is noticed in the commercial PE separator. The PE separator exhibits a remarkable shrinkage after heating at 120 °C for 10 min and totally melted even before one minute as the temperature increased to 150 °C. A shrinkage of about 10% at 150 °C and complete melting at 200 °C with Celgard 2400 reported by Liang et al. demonstrates comparatively excellent dimensional thermostability in PBI-based separators mainly due to the aromatic structure of the membrane.[22] Moreover, the thermal shrinkage of PBI separators at 150 °C is significantly lower than that of high-density polyethylene (HDPE)/alumina nanocomposites fabricated using the extrusion process that can avoid the internal short circuits between two electrodes during battery operation and reduce the risk of thermal runway.[38]

2.4. Porosity and Electrolyte Wettability. The wettability of separators toward the electrolyte has a great influence on the ion conductivity as well as efficient functioning of a battery.[39] The membranes with high porosity (P) can successfully attain high electrolyte uptake and consequently elevated electrochemical performances. The PLAIN PBI separator displays a porosity of about 87% (Table 1). After cross-linking, the porosity (P) has been decreased owing to the chemical bond formed between DBX and PBI. By sharp contrast, the commercial PE separator possesses the lowest porosity of about 40%. To further confirm the wettability of the present membranes, the contact angle toward water and liquid electrolyte is also measured and the results are shown in Figure S3. The PE separator and Celgard 2400 exhibit a relatively high electrolyte contact angle of about 42.8° and 61°, respectively, whereas PBI-based membranes rapidly absorb the electrolyte and exhibit a contact angle between 11° and 14°.[40] As expected from high porosity, the pristine PBI membrane shows an electrolyte uptake of 912% owing to the good compatibility between polar nitrogen in PBI and the electrolyte (Table 1).[41] The cross-linked membranes after CMBA treatment exhibit a high affinity toward both water and electrolyte due to the presence of polar functional groups (carboxyl, −NH).[42] The high electrolyte affinity is an indication of the high Li^+ ion conductivity of the separator.[43] The good electrolyte absorption behavior can also facilitate interfacial compatibility and Li^+ ion diffusion at the electrode/electrolyte interface, which will endow the battery with a poor Ohmic polarization phenomenon and improve cell performance.[40] Moreover, the contact angle of water above 90° on pristine PBI and cross-linked PBI is due to their hydrophobicity, while CMBA treatment supports the hydrophilicity owing to the presence of carboxyl functional groups. The contact angle results confirmed that, regardless of hydrophobicity, the plentiful hydrophilic carboxyl groups and porous structures of CROSSLINK PBI-CMBA could facilitate the absorption and spreading of the liquid electrolyte.

Electrospun PBI separators in this study showed 2 to 2.6 times higher electrolyte uptake than the commercial PE membrane and 10 to 12.8 times than Celgard 2400 reported by Zhu et al.,[40] suggesting that the PBI-based separators could offer more lithium-ion migration during charge/discharge reaction and thereby corresponding battery performance.[12] The CROSSLINK PBI-CMBA exhibits higher electrolyte uptake followed by CROSSLINK PBI and pristine PBI separators. The electrolyte uptake value for PBI-based membranes are similar to that of polyimide (PI) and poly (ethylene-co-vinyl acetate) (EVA)/polyimide (PI)/EVA (PIE) tri-layer membranes (700−1052%) reported by Kim et al.[8] All the above results have unambiguously confirmed superior liquid electrolyte wettability of modified PBI membranes.

2.5. Mechanical Property. The separator must be strong enough to withstand the tension during battery assembly or at unexpected collisions taking place.[12,44] Table 1 and Figure S4 present the mechanical performances of PBI-based and commercial PE separators. The mechanical strength and elongation at break of the PE separator are 32.16 MPa and 174.1%, respectively, suggesting a physical state of the strong and flexible separator. A good separator membrane should have sufficient strength to hinder the Li dendrites and appropriate strain to guarantee flexibility. The PLAIN PBI separator exhibits tensile strength and modulus of 3.61 and 22.25 MPa, respectively. After cross-linking, both the strength and modulus were increased up to 10.77 and 36.33 MPa, respectively, due to the strong chemical network formed among PBI chains through DBX. However, the highly porous structure formed after CMBA modifications leads to the deterioration in the mechanical property of the cross-linked PBI membrane.[23] The tensile strength value achieved is similar to the porous PBI-based separator reported by Liang et al.[22] Furthermore, the PBI separators are mechanically weaker than the commercial PE due to the difference in the manufacturing process. PE film used in this study was manufactured by an optimized wet process, including an extrusion step, two axis elongation, and a pore generation step via solvent extraction to control thickness, pore structure, as well as mechanical strength.[33,45] Even though the mechanical properties are relatively lower than those of the commercial PE separator and Celgard 2400,[22] the present membranes can be randomly stretched and folded, which can still meet the requirements for commercialization.

https://doi.org/10.1021/acsomega.2c05472
ACS Omega 2022, 7, 47784−47795

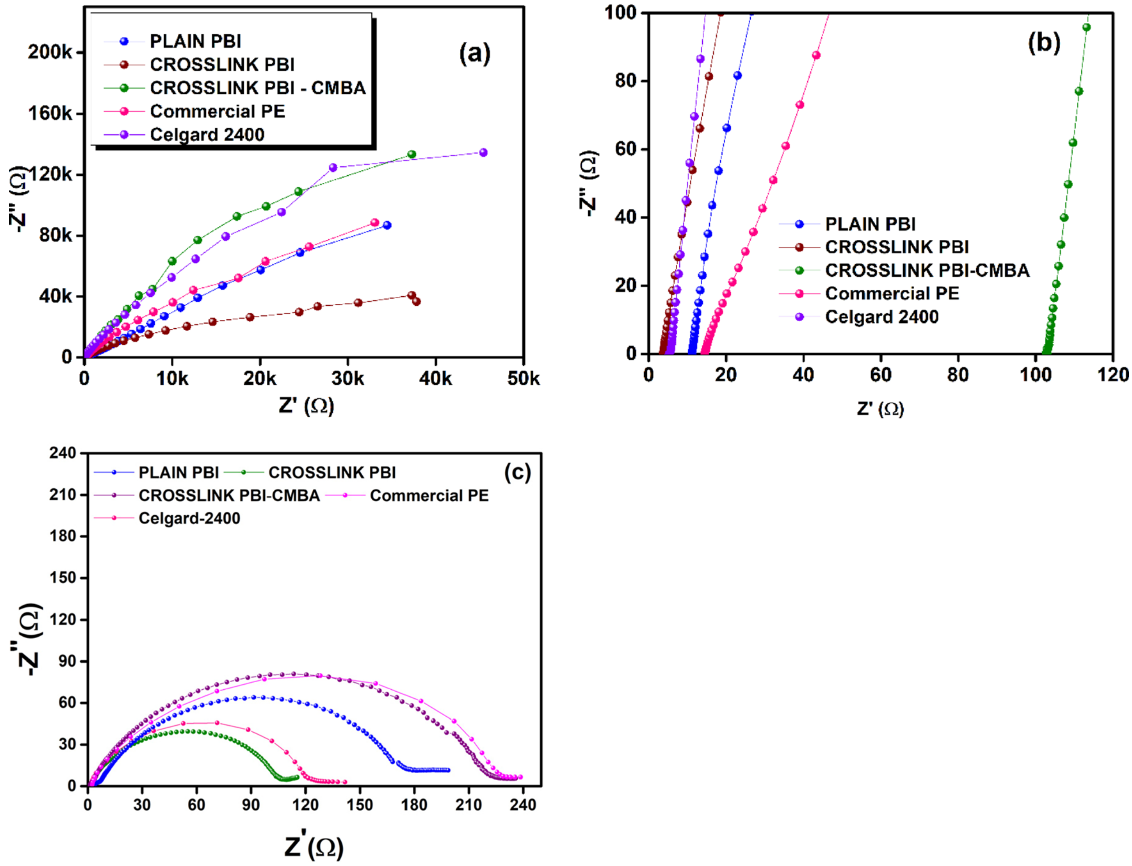

Figure 5. Electrochemical impedance spectra of (a,b) the SS/separator/SS cell and (c) the Li/separator/Li cell with different separators: PLAIN PBI, CROSSLINK PBI, CROSSLINK PBI-CMBA, commercial PE, and Celgard 2400.

2.6. Electrochemical Performances.

2.6.1. Ionic Conductivity. The ionic conductivity of the separator has a significant role in achieving high rate capability and battery reversibility performances.[3,46] According to the Nyquist plot obtained in Figure 5a,b, the bulk resistance (intercept of the X-axis of the plot) and ionic conductivity of all the PBI-based membranes are calculated and the values are illustrated in Table 2. It can be noticed that the maximum ionic conductivity of 0.86 mS cm^{-1} is obtained for CROSSLINK PBI membrane, 1.2 times more than that of Celgard 2400 (0.687 mS cm^{-1}) and 3.8 times more than that of the commercial PE separators (0.228 mS cm^{-1}), assigned to its higher porosity and electrolyte uptake. The strong interaction of the electron-rich imidazole ring on PBI with lithium ions also aids the lithium salt dissociation into Li^+ ions by strong conjugated interactions and more easy ion transmission.[36,41] Even though the CMBA-treated membranes exhibited higher porosity and wettability with liquid electrolytes, the CROSSLINK PBI membrane shows comparatively high conductivity due to the higher flexibility and the presence of Br^- ions in its structure, which facilitate easy Li^+ ion conduction. The polarizability of the anion (Br^-) allows for the hopping-site environment to reduce the activation barriers and facilitate easy ion conduction. Kraft et al. have shown the influence of anion polarizability on the lattice stiffness and the associated Li^+ ion migration in their studies.[47]

Table 2. Electrochemical Performances of Different Separators

separator designation	thickness (mm)	bulk resistance (Ω)	ionic conductivity (σ) (mS cm^{-1})	tortuosity (τ)
PLAIN PBI	0.058	11.30	0.654	3.61
CROSSLINK PBI	0.025	3.70	0.860	2.82
CROSSLINK PBI-CMBA	0.032	102.92	0.396	4.39
commercial PE	0.025	14.52	0.228	4.15
Celgard 2400	0.027	5.01	0.687	2.42

The high ionic conductivity may improve the charge—discharge capacity and thus decrease the rate of increase of the transfer resistance in the cycle test.[3,48] To study the impact of membranes' internal pores connectivity on conductivity, tortuosity values are calculated, and the values are illustrated in Table 2. Even though numerous pores are present in the membranes, the interconnectivity of pores is necessary for good Li-ion passage. CROSSLINK PBI shows that the lowest proper tortuosity (2.82) among other PBI-based membranes revealed its applicability to the energy storage devices.[36] CROSSLINK PBI-CMBA exhibited a maximum tortuosity value of about 4.39 and showed the prolonged lithium-ion path through the membrane. Tortuosity, membranes' internal pore connectivity, is a diffusional parameter describing the complexity of mass or ionic transport that affects transport parameters, liquid-phase diffusivity, and conductivity. The Li^+ ion transportation path will be extended with an increase in tortuosity. If the pore size and connectivity of a nonwoven separator are not sufficiently controlled, critical problems such as nonuniform current acceleration, internal short circuit, mitigation of liquid electrolyte leakage, and self-discharge of the batteries may occur.[33,49,50]

https://doi.org/10.1021/acsomega.2c05472
ACS Omega 2022, 7, 47784−47795

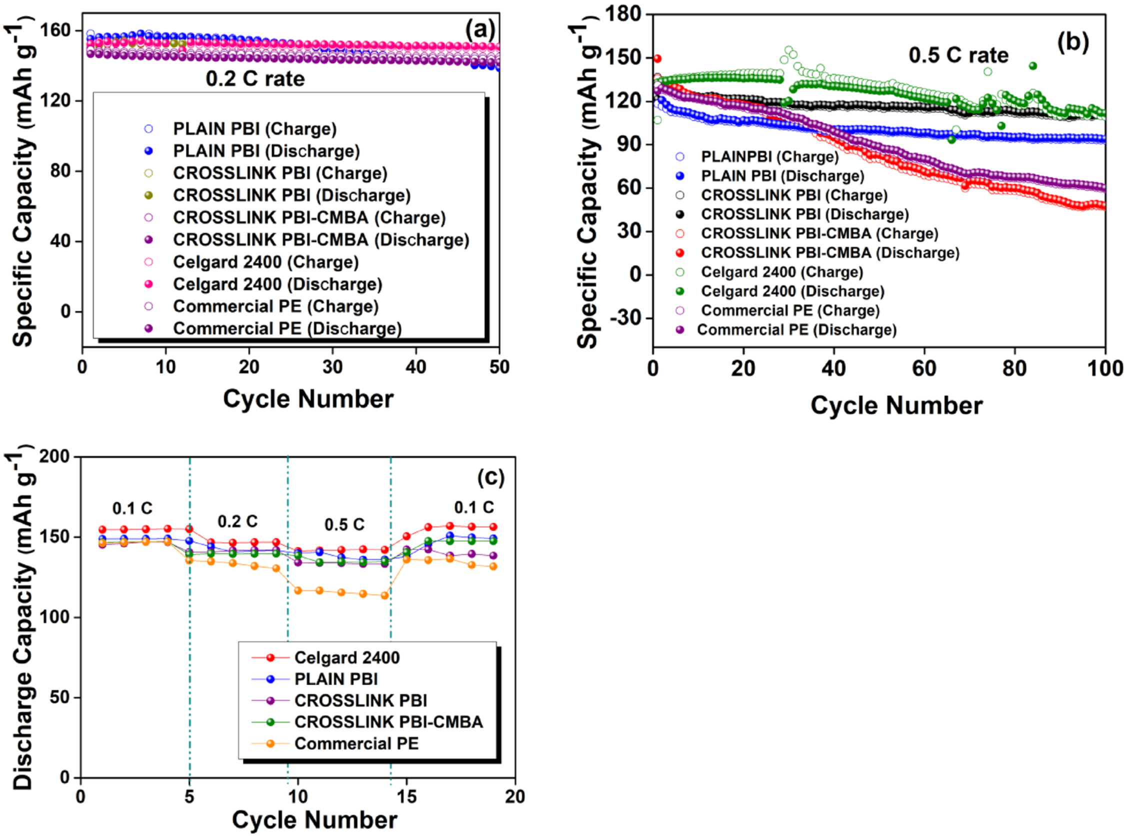

Figure 6. Cyclic stability of batteries with different separators at (a) 0.2 C and (b) 0.5 C; (c) comparison of rate performance of batteries with different separators.

The interfacial compatibility between the electrode and the polymer separator was also measured using ac impedance spectroscopy of the Li/separator/Li cell and the results are displayed in Figure 5c. A small semicircle related to the solid electrolyte interphase (SEI)-derived resistance and a clear decrease for the second semicircle that relates to charge transfer resistance can be observed for the CROSSLINK PBI separator-based cell. The charge transfer resistance deduced from the semi-circle in the high-frequency region is about 106.5 Ω and 120.7 Ω for CROSSLINK PBI and Celgard-2400, respectively. The lower interfacial impedance that existed between the CROSSLINK PBI separator and the lithium electrode reflects the interfacial compatibility between the separator and the Li metal electrode, which is ascribed to the good electrolyte absorption behavior of the separator that can facilitate Li^+ diffusion at the separator−electrode interface and greatly help improve the overall cell performance.[40,51,52]

2.6.2. Battery Performance. The cell performance of the separators using $LiFePO_4$/Li half-cells at 0.2 and 0.5 C rates at room temperature is illustrated in Figures S5 and 6a,b. All the cells assembled with different separators display stable charge−discharge platforms, indicating its remarkable reversibility.[53] The battery with the CROSSLINK PBI separator has the best cycling performance among all the other PBI separator-based batteries. The cell with the PLAIN PBI separator reveals an initial charge capacity of 158.3 mAh g^{-1}, a discharge capacity of 155.2 mAh g^{-1}, and a Coulombic efficiency of 98.04% at 0.2 C rate. After 50 cycles, the cell maintained a Coulombic efficiency of 99.8% (charge and discharge capacities of 139.0 and 138.7 mAh g^{-1}). As observed in Figures 6a and S5, the 0.2 C discharge capacities of the battery assembled with CROSSLINK PBI as well as CMBA-treated CROSSLINK PBI are 151.4 and 147.8 mAh g^{-1} respectively. CROSSLINK PBI exhibits a Coulombic efficiency of 99.8% even after 50 charge−discharge cycles, which is superior to the value of the cell using commercial PE and Celgard 2400 separators. The discharge capacity after 50 cycles of charging and discharging corresponds to 88.4% of the theoretical value of $LiFePO_4$ (170 mAh g^{-1}).[12] As the C rate increases to 0.5, the PLAIN PBI membrane maintained a Coulombic efficiency of 96.5% (charge capacity: 120.7 mAh g^{-1}; discharge capacity: 116.5 mAh g^{-1}) and 99% (charge capacity: 94.0 mAh g^{-1}; discharge capacity: 93.1 mAh g^{-1}), respectively, after the first and the 100th cycle of charging−discharging. CROSSLINK PBI exhibits a maximum efficiency of about 99% after the 100th charge−discharge cycle, which is superior to the commercial PE and Celgard 2400 separators. A fast capacity decay while cycling at 0.5 C rate is observed for the CROSSLINK PBI−CMBA separator (Figure 6b) as a result of low ionic conductivity and high tortuosity values.[36] The remarkable cycling performance of the CROSSLINK PBI separator is attributed to the synergistic effects of its excellent electrolyte uptake, flexibility, and electrochemical stability, which could facilitate easy ion migration, electrolyte retention, and reduction in interfacial resistance while cycling.

The rate capability of the cells containing different separators are investigated at room temperature and different charge−discharge current densities from 0.1 to 0.5 C for 20 cycles and the discharge capacities of the cells are shown in Figure 6c. All separators were continuously cycled for five cycles at each rate and the rate was reduced back to 0.1 C. A slow attenuation in the discharge capacities with an increase in current density is observed, attributed to the increase of the Ohmic polarization

https://doi.org/10.1021/acsomega.2c05472
ACS Omega 2022, 7, 47784−47795

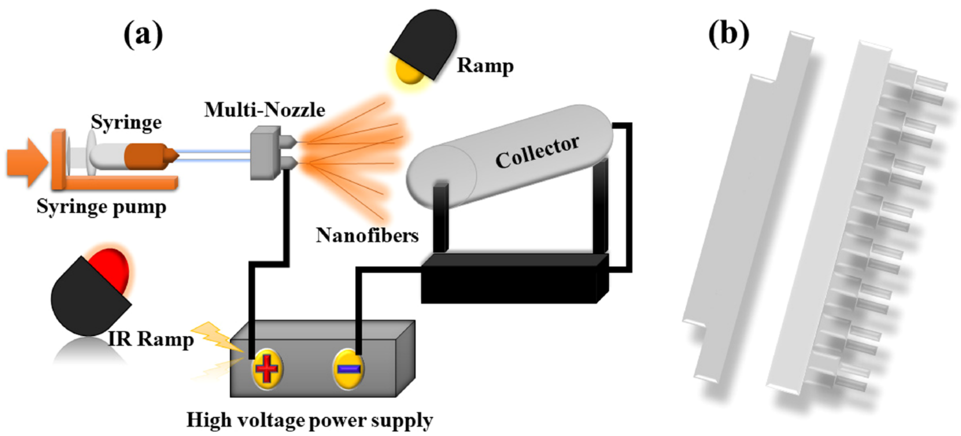

Figure 7. Schematic of (a) electrospinning device and (b) multi-nozzle.

effect and overcharging potential at higher current density.[12] Initially, at very low current density, no significant changes were noticed in the performance of various PBI-based separators. The cell with a CROSSLINK PBI separator shows the highest discharge capacity at the same current density of 0.2 C, attributed to its high ion conductivity and superior compatibility at the electrode/separator interface.[54] The cell assembled with CROSSLINK PBI yields about 92.4% of the initial capacity at a high discharge rate (0.5 C). In addition to its improved cycling performance, the CROSSLINK PBI separator also displayed high rate performance with a discharge capacity of 145.2, 140.7, and 133.8 mAh g^{-1} at 0.1, 0.2, and 0.5 C, respectively. When the battery was cycled back to 0.1 C, a high capacity of 142.2 mAh g^{-1} was retained (97.9%), which indicates the high reversibility of the battery. For comparison, PLAIN PBI, CROSSLINK PBI-CMBA, commercial PE, and Celgard 2400 separators hold 92.6, 95.8, 93.0, and 97.3%, respectively. The outstanding performances of the PBI-based separators are due to their high porosity, electrolyte wettability and ion conductivity.

3. SUMMARY AND CONCLUSIONS

Currently, polyolefin as a secondary battery separator is the most commercialized because of its lower price and high mechanical as well as chemical properties. However, the low thermal stability, low porosity, and poor electrolyte uptake limited their applications. To improve these shortcomings, polybenzimidazole, a high-temperature, highly durable super engineering material-based membranes are fabricated using the electrospinning process. A multi-nozzle is used to increase productivity and form a fine porous structure. Good coverage over a large area demonstrates prospects for scale up. Better process controllability in the multi-nozzle design leads to good-quality (size, distribution) fibers which avoid undesired short circuit of cells during charging/discharging. Cross-linking of PBI is done using α, α'-dibromo-m-xylene (DBX) to improve the mechanical as well as chemical stability and hydrophilization using 4-(chloromethyl) benzoic acid (CMBA) to further improve electrolyte wettability. Compared to the commercial PE separator and Celgard 2400, CROSSLINK PBI and CROSSLINK PBI-CMBA exhibits excellent thermal stability which would help enhance battery safety. More significantly, the introduction of CMBA treatment was found to deliver the enhancement of porosity and electrolyte uptake (1151%). However, their high tortuosity and low conductivity values adversely affected the battery cycling stability. The CROSSLINK PBI membrane exhibits superior ionic conductivity of about 0.860 mS cm^{-1}. Meanwhile, the stable Coulombic efficiency along with high-capacity retention (97.9%) after being cycled back to lower C rate demonstrates the excellent cyclic stability and high reversibility of battery. Therefore, our study provides an effective strategy to design the thermally stable separator for high-power lithium metal batteries.

4. EXPERIMENTAL SECTION

4.1. Materials. The materials used for this study included liquid-type polybenzimidazole (S26, PBI advanced materials, Korea), *N*, *N*-dimethyl acetate (DMAc, Sigma Aldrich), α, α'-dibromo-m-xylene (DBX, 97%, Sigma Aldrich), 4-(chloromethyl) benzoic acid (CMBA, 95%, Sigma Aldrich), sodium persulfate (≥98, Sigma Aldrich), acetone (Sigma Aldrich), acrylonitrile (AN, >99%; Samchun), and isopropyl alcohol (IPA, ≥98%, Sigma Aldrich). All chemicals were used without any further purification. A commercial polyethylene (PE) separator (25 μm thick) supplied by W-Scope Korea Co., Ltd. and polypropylene (PP) (Celgard 2400, USA) membrane were used for comparative study. *N*-methyl pyrrolidone (NMP), lithium iron phosphate ($LiFePO_4$), poly(vinylidene fluoride) (PVDF), and cathode materials were provided by Sigma Aldrich. Lithium metal (Honjo metal Co., Ltd.) was used as the anode and 1 M lithium hexafluorophosphate solution ($LiPF_6$) in ethylene carbonate/diethyl carbonate (EC/DEC) (1,1, v/v) (Sigma-Aldrich) was used as the electrolyte. The cell test was conducted using a Swagelok cell (Hi-Touch, Korea).

4.2. Electrospinning Using the Multi-Nozzle. A schematic of the electrospinning device is shown in Figure 7a. The electrospinning device consists of a collector connected to the electric charge supply (Tekham, Korea), a syringe pump (Havard, USA) to control the speed of spinning solution feed, a multi-nozzle connected to the syringe, and 23 gauge needles to the multi-nozzle. Moreover, an infrared (IR) lamp (220 V, 60 W) for controlling temperature and humidity inside the housing and an illuminated lamp for visual inspection of fiber were also used. The collector was wrapped with an aluminum foil or a PTFE nonwoven fabric (Namyang non-woven fabric Co., Ltd) to facilitate the acquisition of electrospun fibers. A male−female fitting metal nozzle-PTFE tube (1/16′ size) (Nano NC, Korea) was used to inject the spinning solution. The multi-nozzle was divided into a distribution part consisting of 16 holes and an injection part to inject the polymeric solution (Figure 7b). In this experiment, 23 G metal needles were inserted into eight

https://doi.org/10.1021/acsomega.2c05472
ACS Omega 2022, 7, 47784−47795

holes excluding four edges of the multi-nozzle to manufacture PBI fibers. The 8−3 holes on the edges were blocked with Teflon to prevent the solution flow. The injection syringe was connected to the PTFE tube (1/16′size).

4.3. Preparation of PBI Separators. PBI-based separators were fabricated by the electrospinning method with a steady flow rate of 1.1 mL h^{-1} and a high voltage of approximately 22 kV using the multi-nozzle as per the scheme illustrated in Figure 7. PBI solution with different concentrations (14, 15, 16, 17, and 18 wt %) was prepared by dissolving PBI in DMAc by stirring at 80 °C for 24 h using an oil bath. Then, the resultant solution was loaded into the syringe and vacuum-degassed for about 24 h to remove air bubbles and subjected to IR radiation for 30 to 60 min before electrospinning to maintain a constant temperature (40 °C) and humidity (∼20%) inside the housing. The needle to collector distance was 15 cm. The obtained electrospun membranes were dried in an oven at ambient temperature (25 °C) for 24 h.

4.4. Modification of the PBI Separator: Cross-Linking and CMBA Hydrophilization. α, α'-Dibromo-m-xylene (DBX) solution (3 wt %) in acrylonitrile was used as the cross-linking solution. The PBI membrane was treated with the cross-linking agent by stirring the membrane in solution at 80 °C for 24 h. Afterward, the cross-linked membrane was immersed in isopropanol (IPA) for about 24 h to remove the residual material followed by drying in a vacuum oven (OV-11, Jeio Tech) at 60 °C for 24 h. The cross-linked membrane was designated as CROSSLINK PBI, and the mechanism of cross-linking is shown in Figure S1.[34]

The cross-linked membrane was then treated with 4-(chloromethyl) benzoic acid (CMBA) to activate the surface and improve its electrolyte wettability. CMBA solution (0.5 wt %) in acetone was used as the hydrophilization agent and sodium persulfate as the free radical initiator for CMBA activation. The cross-linked PBI membrane was immersed in sodium persulfate solution (1 wt % in distilled water), and then, CMBA/acetone solution was added slowly. As CMBA is insoluble in water, care should be taken during addition to prevent precipitation. The reaction was then carried out at 40 °C for 24 h. This temperature was selected to minimize solvent evaporation.[55] After the reaction, the modified PBI membrane was immersed in acetone for 24 h to remove CMBA and then in deionized water for another 24 h to remove any remaining sodium persulfate and acetone. Finally, the modified membrane was dried at 60 °C for 24 h using a vacuum oven. The chemical structure of the cross-linked PBI after hydrophilization with CMBA (CROSSLINK PBI-CMBA) is shown in Figure 8. Table 3 presents the designation of three different separators used in this study.

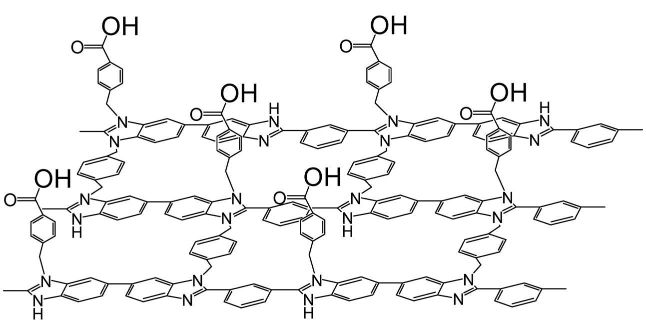

Figure 8. Chemical structure of cross-linked CMBA-treated PBI.

Table 3. Designation of Separators

sample designation	treatment method
PLAIN PBI	electrospun pristine PBI
CROSSLINK PBI	cross-linked electrospun PBI
CROSSLINK PBI-CMBA	CMBA-treated cross-linked PBI

4.5. Characterization. Scanning electron microscopy (SEM, Phillips XL30 S FEG, Netherlands) with an electron beam of accelerating voltage 15 kV was used to investigate the surface morphology of the separators. Before the examination, the samples were sputter-coated (JEOL JFC-110 E) with gold to avoid charge accumulation. The average diameter of the nanofibers was obtained using the ImageJ software (NIH, USA) by counting 50 randomly selected nanofibers from the SEM images.[12] The chemical structures of different separators were confirmed by using Fourier transform infrared (FTIR) spectroscopy with attenuated total reflectance (Nicolet Impact 400, Thermo Scientific, USA) at room temperature, in the wavenumber range of 600−4000 cm^{-1} with a resolution of 4 cm^{-1} and 64 scans. The water and electrolyte (1 M $LiPF_6$ in EC/DMC = 1/1 (v/v)) contact angles were determined using a Phoenix 300 Touch contact angle analyzer (Surface Electro-Optics Ltd) at 25 °C. Mechanical properties of the membranes were measured using a universal testing machine (UTM, Zwick Tensile machine) at a cross-head speed of 10 mm min^{-1}, and the sample was in the form of a dog bone. The average of three samples was reported. The thermal stability of the membranes from room temperature to 700 °C was investigated using a thermogravimetric analyzer (TGA, Q50, TA Instruments, USA) at a heating rate of 10 °C min^{-1} in a nitrogen atmosphere. Furthermore, the thermal shrinkage of the separators was examined by measuring the dimensional change after placing 16 π coin cell samples in an oven at 150 °C for 30 min.

The porosity (P) of the PBI separator and the commercial PE separator was measured by the n-butanol immersion method. The dry separators (2 cm × 1 cm × 30 μm) were soaked in n-butanol for 2 h at room temperature, and porosity was calculated using the following eq 1:

$$\text{Porosity, } P\ (\%) = \frac{W_w - W_d}{\rho_b V_d} \tag{1}$$

where W_d and W_w are the weights of the samples (accuracy: ± 0.01 mg) before and after soaking in n-butanol, respectively. ρ_b and V_d are, respectively, the density of n-butanol and the volume of the dry sample. An average of three specimens was reported.

The electrolyte uptake (EU) was measured by measuring the weight of the separators (2 cm × 2 cm) before and after soaking in the liquid electrolyte (1 M $LiPF_6$ in EC/DMC = 1/1 (v/v)) for 2 h. The electrolyte uptake was calculated using the formula 2:

$$\text{EU } (\%) = \frac{W_2 - W_1}{W_1} \times 100 \tag{2}$$

where W_2 is the weight of the separator after being immersed in the electrolyte and W_1 is the weight of the dry separator. An average of three specimens was reported.

The electrochemical impedance spectroscopy (EIS) (ZIVE SP2, WonA Tech. Co.) measurements were used to calculate the ionic conductivity by placing the electrolyte-soaked separator between two stainless-steel electrodes. The measurements were

https://doi.org/10.1021/acsomega.2c05472
ACS Omega 2022, 7, 47784−47795

taken at an ac voltage of 5 mV in a frequency range of 2 MHz to 0.1 Hz. The ionic conductivity (σ) was calculated using eq 3:

$$\sigma = \frac{d}{R_b \times A} \quad (3)$$

where A and d are the area and thickness (using a Vernier caliper, accuracy: ± 0.01 mm) of the separator, respectively. R_b is the bulk resistance of the separator determined from the Nyquist plot. In the same way, the Nyquist plot of the Li/separator/Li cell with Celgard, PE, as well as PBI-based separators and lithium metal as two electrodes in the frequency range of 0.1 Hz to 1 MHz was also gained by using EIS.

The tortuosity of all the membranes was calculated from porosity and conductivity values using eq 4:

$$\text{Tortuosity } (\tau) = \sqrt{\frac{P\sigma_0}{\sigma}} \quad (4)$$

where P is the porosity of the membrane, σ_0 is the conductivity of the pure liquid electrolyte (9.8 mS cm^{-1}), and σ is the conductivity of the separator at room temperature.[36,56]

Battery performance was analyzed using Swagelok cells assembled by sandwiching the liquid electrolyte-soaked separator between the cathode and anode in a glovebox filled with the argon atmosphere. The cathode slurry was prepared by mixing 80 wt % $LiFePO_4$, 10 wt % poly(vinylidene fluoride) (PVDF), and 10 wt % super-P (SP) carbon with the NMP solvent. The slurry was uniformly curtain-coated onto the aluminum foil. Lithium metal was used as the anode. The liquid electrolyte consisted of 1 M $LiPF_6$ dissolved in the EC/DEC (1:1 volume ratio) mixture. For comparison, a cell with the same electrolyte and electrode was also assembled using a commercial PE separator and PP (Celgard 2400). The thickness of the separators and mass loading of the LFP cathode was varied from 0.025 to 0.058 mm and 1.7 to 2.2 mg, respectively. The performance of the membranes as a separator was studied by measuring the rate capability at different charge/discharge current densities (0.1 to 0.5 C rate) and cycle performance in the voltage range of 2.0 to 4.2 V under constant current (0.2 and 0.5 C).

■ ASSOCIATED CONTENT

Supporting Information

The Supporting Information is available free of charge at https://pubs.acs.org/doi/10.1021/acsomega.2c05472.

Cross-linking mechanism; contact angle; stress−strain curves; and battery performance (PDF)

■ AUTHOR INFORMATION

Corresponding Author

Sang Yong Nam − *Department of Materials Engineering and Convergence Technology and Research Institute for Green Energy Convergence Technology, Gyeongsang National University, Jinju 52828, Republic of Korea;* orcid.org/0000-0002-6056-2318; Email: walden@gnu.ac.kr

Authors

Ji Hye Jung − *Department of Materials Engineering and Convergence Technology, Gyeongsang National University, Jinju 52828, Republic of Korea*

Vijayalekshmi Vijayakumar − *Research Institute for Green Energy Convergence Technology, Gyeongsang National University, Jinju 52828, Republic of Korea*

Anupriya K. Haridas − *Department of Materials Engineering and Convergence Technology, Gyeongsang National University, Jinju 52828, Republic of Korea;* Present Address: Department of Engineering, King's College London, Strand WC2R 2LS, U.K; orcid.org/0000-0002-1016-5701

Jou-Hyeon Ahn − *Department of Materials Engineering and Convergence Technology and Department of Chemical Engineering, Gyeongsang National University, Jinju 52828, Republic of Korea*

Complete contact information is available at: https://pubs.acs.org/10.1021/acsomega.2c05472

Author Contributions

⊥J.H.J. and V.V. contributed equally to this work.

Notes

The authors declare no competing financial interest.

■ ACKNOWLEDGMENTS

This work was supported by the Technology Innovation Program (or Material parts technology development-Material parts package program) (10080703, highly durable and heat-resistant polybenzimidazole material) funded by the Ministry of Trade, Industry & Energy (MOTIE, Korea). This research was also supported by the Basic Science Research Program through the National Research Foundation of Korea (NRF) funded by the Ministry of Education (NRF−2020R1A6A1A03038697).

■ REFERENCES

(1) Wang, X.; Hao, X.; Hengjing, Z.; Xia, X.; Tu, J. 3D Ultraviolet polymerized electrolyte based on PEO modified PVDF-HFP electrospun membrane for high-performance lithium-sulfur batteries. *Electrochim. Acta* **2020**, *329*, No. 135108.

(2) Lin, Y.; Pitcheri, R.; Zhu, J.; Jiao, C.; Guo, Y.; Li, J.; Qiu, Y. Electrospun PVDF/PSSLi ionomer films as a functional separator for lithium-sulfur batteries. *J. Alloys Compd.* **2019**, *785*, 627−633.

(3) Dong, T.; Arifeen, W. U.; Choi, J.; Yoo, K.; Ko, T. Surface-modified electrospun polyacrylonitrile nano-membrane for a lithium-ion battery separator based on phase separation mechanism. *Chem. Eng. J.* **2020**, *398*, No. 125646.

(4) Yao, H.; Yan, K.; Li, W.; Zheng, G.; Kong, D.; Seh, Z. W.; Narasimhan, V. K.; Liang, Z.; Cui, Y. Improved lithium-sulfur batteries with a conductive coating on the separator to prevent the accumulation of inactive S-related species at the cathode-separator interface. *Energy Environ. Sci.* **2014**, *7*, 3381−3390.

(5) Yang, Y.; Yuan, W.; Zhang, X.; Yuan, Y.; Wang, C.; Huang, Y. Y.; Qiu, Z.; Tang, Y. Overview on the applications of three-dimensional printing for rechargeable lithium-ion batteries. *Appl. Energy* **2020**, *257*, No. 114002.

(6) Xu, K.; Qin, Y.; Xu, T.; Xie, X.; Deng, J.; Qi, J.; Huang, C. Combining polymeric membranes with inorganic woven fabric: Towards the continuous and affordable fabrication of a multifunctional separator for lithium-ion battery. *J. Membr. Sci.* **2019**, *592*, No. 117364.

(7) Song, Q.; Li, A.; Shi, L.; Qian, C.; Feric, T. G.; Fu, Y.; Zhang, H.; Li, Z.; Wang, P.; Li, Z.; Zhai, H.; Wang, X.; Dontigny, M.; Zaghib, K.; Park, A. H.; Myers, K.; Chuan, X.; Yang, Y. Thermally stable, nano-porous and eco-friendly sodium alginate/attapulgite separator for lithium-ion batteries. *Energy Storage Mater.* **2019**, *22*, 48−56.

(8) Kim, S.; Kwon, M. S.; Han, J. H.; Yuk, J.; Lee, J. Y.; Lee, K. T.; Kim, T. H. Poly(Ethylene-Co-Vinyl Acetate)/Polyimide/Poly(ethylene-co-vinyl acetate) tri-layer porous separator with high conductivity and tailored thermal shutdown function for application in sodium-ion batteries. *J. Power Sources* **2021**, *482*, No. 228907.

(9) Ding, L.; Zhang, C.; Wu, T.; Yang, F.; Lan, F.; Cao, Y.; Xiang, M. Effect of temperature on compression behavior of polypropylene

separator used for lithium-ion battery. *J. Power Sources* **2020**, *466*, No. 228300.
(10) Costa, C. M.; Lizundia, E.; Lanceros-Mendez, S. Polymers for advanced lithium-ion batteries: State of the art and future needs on polymers for the different battery components. *Prog. Energy Combust. Sci.* **2020**, *79*, No. 100846.
(11) Zhang, S. S. A review on the separators of liquid electrolyte Li-ion batteries. *J. Power Sources* **2007**, *164*, 351−364.
(12) Huang, C.; Ji, H.; Yang, Y.; Guo, B.; Luo, L.; Meng, Z.; Fan, L.; Xu, J. TEMPO-oxidized bacterial cellulose nanofiber membranes as high-performance separators for lithium-ion batteries. *Carbohydr. Polym.* **2020**, *230*, No. 115570.
(13) Kim, J. Y.; Lim, D. Y. Surface-modified membrane as a separator for lithium-ion polymer battery. *Energies* **2010**, *3*, 866−885.
(14) Lee, Y. M.; Kim, J. W.; Choi, N. S.; Lee, J. A.; Seol, W. H.; Park, J. K. Novel porous separator based on PVdF and PE non-woven matrix for rechargeable lithium batteries. *J. Power Sources* **2005**, *139*, 235−241.
(15) Wang, H.; Huang, H.; Wunder, S. L. Novel microporous poly(vinylidene fluoride) blend electrolytes for lithium-ion batteries. *J. Electrochem. Soc.* **2000**, *147*, 2853−2861.
(16) Chen, L.; Shaw, L. L. Recent Advances in lthium-sulfur batteries. *J. Power Sources* **2014**, *267*, 770−783.
(17) Safa, M.; Hao, Y.; Chamaani, A.; Adelowo, E.; Chawla, N.; Wang, C.; El-Zahab, B. Capacity fading mechanism in lithium-sulfur battery using poly(ionic liquid) gel electrolyte. *Electrochim. Acta* **2017**, *258*, 1284−1292.
(18) Van Krevelen, D. W. New developments in the field of flame-resistant fibres. *Angew. Makromol. Chem.* **1972**, *22*, 133−157.
(19) Vogel, H.; Marvel, C. S. Polybenzimidazoles, New thermally stable polymers. *J. Polym. Sci., Part A: Polym. Chem.* **1996**, *34*, 1125−1153.
(20) Rowlands, R. J. Comfort properties of blankets: Part I: Measurement of thermal conductivity. *Text. Res. J.* **1963**, *33*, 343−350.
(21) Sun, G.; Kong, L.; Liu, B.; Niu, H.; Zhang, M.; Tian, G.; Qi, S.; Wu, D. Ultrahigh-strength, nonflammable and high-wettability separators based on novel polyimide-Core@polybenzimidazole-sheath nanofibers for advanced and safe lithium-ion batteries. *J. Membr. Sci.* **2019**, *582*, 132−139.
(22) Liang, N.; Fang, J.; Guo, X. A simple approach for preparation of porous polybenzimidazole membranes as a promising separator for lithium ion batteries. *J. Mater. Chem. A* **2017**, *5*, 15087−15095.
(23) Li, H.; Zhang, B.; Lin, B.; Yang, Y.; Zhao, Y.; Wang, L. Electrospun poly (ether ether ketone) nanofibrous separator with superior performance for lithium-ion batteries. *J. Electrochem. Soc.* **2018**, *165*, A939−A946.
(24) Chen, H.; Ning, J. X. Preparation and characterization of polyvinylidene fluoride/octaphenyl-polyhedral oligomeric silsesquioxane hybrid lithium-ion battery separators by electrospinning. *Solid State Ionics* **2017**, *310*, 134−142.
(25) Hsieh, C. T.; Lin, S. C.; Lee, C. H.; Liu, C. F.; Hu, C. C. Designing multifunctional polyethylene-polyimide composite separators for rechargeable lithium-ion batteries. *J. Electrochem. Soc.* **2019**, *166*, A3132−A3138.
(26) Pai, J. Y.; Hsieh, C. T.; Lee, C. H.; Wang, J. A.; Ku, H. Y.; Huang, C. L.; Hardwick, L. J.; Hu, C. C. Engineering of electrospun polyimide separators for electrical double-layer capacitors and lithium-ion cells. *J. Power Sources* **2021**, *482*, No. 229054.
(27) Pai, J. Y.; Ku, H. Y.; Lin, C. C.; Chiang, C. W.; Hardwick, L. J.; Hu, C. C. Porous polyimide separator promotes uniform lithium plating for lithium-free cells. *Electrochem. Sci. Adv.* **2022**, *2*, No. e2100091.
(28) Xiao, W.; Song, J.; Huang, L.; Yang, Z.; Qiao, Q. PVA-ZrO_2 multilayer composite separator with enhanced electrolyte property and mechanical strength for lithium-ion batteries. *Ceram. Int.* **2020**, *46*, 29212−29221.
(29) Pelach, M. A.; Delgado-Aguilar, M.; Alcala, M.; Puig, J.; Blanco, A.; Mutje, P. New strategy for the production of packaging from recycled fibers. *Cellul. Chem. Technol.* **2016**, *50*, 449−454.
(30) Stanger, J.; Staiger, M. P.; Tucker, N.; Coles, S. R.; Jacobs, D.; Kirwan, K. Effect of charge density on the taylor cone in electrospinning. *Solid State Phenom.* **2009**, *151*, 54−59.
(31) Yarin, A. L.; Koombhongse, S.; Reneker, D. H. Taylor cone and jetting from liquid droplets in electrospinning of nanofibers. *J. Appl. Phys.* **2001**, *90*, 4836−4846.
(32) Parreno, R. P.; Liu, Y. L.; Beltran, A. B.; Carandang, M. B. Effect of a direct sulfonation reaction on the functional properties of thermally-crosslinked electrospun polybenzoxazine (PBz) nanofibers. *RSC Adv.* **2020**, *10*, 14198−14207.
(33) Lee, Y.; Park, J.; Jeon, H.; Yeon, D.; Kim, B. H.; Cho, K. Y.; Ryou, M. H.; Lee, Y. M. In-depth correlation of separator pore structure and electrochemical performance in lithium-ion batteries. *J. Power Sources* **2016**, *325*, 732−738.
(34) Valtcheva, I. B.; Marchetti, P.; Livingston, A. G. Crosslinked polybenzimidazole membranes for organic solvent nanofiltration (OSN): Analysis of crosslinking reaction mechanism and effects of reaction parameters. *J. Membr. Sci.* **2015**, *493*, 568−579.
(35) Yuan, M.; Liu, K. Rational design on separators and liquid electrolytes for safer lithium-ion batteries. *J. Energy Chem.* **2020**, *43*, 58−70.
(36) Hussain, A.; Li, D.; Luo, Y.; Zhang, H.; Zhang, H.; Li, X. Porous membrane with improved dendrite resistance for high-performance lithium metal-based battery. *J. Membr. Sci.* **2020**, *605*, No. 118108.
(37) Fishel, K. J.; Gulledge, A. L.; Pingitore, A. T.; Hoffman, J. P.; Steckle, W. P.; Benicewicz, B. C. Solution polymerization of polybenzimidazole. *J. Polym. Sci., Part A: Polym. Chem.* **2016**, *54*, 1795−1802.
(38) Lee, C. H.; Huang, Y. C.; Kinzlinger, U.; Esken, D.; Lin, Y. H.; Tsai, A. T.; Wu, H. C.; Li, Y. C.; Hu, C. C. A novel cavity-enhanced polyethylene/nanostructured-alumina separator with long cycle life and high rate capability for advanced lithium-ion batteries. *ACS Sustainable Chem. Eng.* **2021**, *9*, 1590−1598.
(39) Li, Y.; Wang, W.; Liu, X.; Mao, E.; Wang, M.; Li, G.; Fu, L.; Li, Z.; Eng, A. Y. S.; Seh, Z. W.; Sun, Y. Engineering stable electrode-separator interfaces with ultrathin conductive polymer layer for high-energy-density Li-S batteries. *Energy Storage Mater.* **2019**, *23*, 261−268.
(40) Zhu, C.; Zhang, J.; Xu, J.; Yin, X.; Wu, J.; Chen, S.; Zhu, Z.; Wang, L.; Wang, H. Aramid nanofibers/polyphenylene sulfide nonwoven composite separator fabricated through a facile papermaking method for lithium ion battery. *J. Membr. Sci.* **2019**, *588*, No. 117169.
(41) Liu, X.; Zhang, B.; Wu, Y.; Chen, J.; Fang, M.; Wang, L.; Wang, L. The effects of polybenzimidazole nanofiber separator on the safety and performance of lithium-ion batteries: Characterization and analysis from the perspective of mechanism. *J. Power Sources* **2020**, *475*, No. 228624.
(42) Sheng, L.; Song, L.; Gong, H.; Pan, J.; Bai, Y.; Song, S.; Liu, G.; Wang, T.; Huang, X.; He, J. Polyethylene separator grafting with polar monomer for enhancing the lithium-ion transport property. *J. Power Sources* **2020**, *479*, No. 228812.
(43) Zhu, W.; Zhang, Z.; Wei, J.; Jing, Y.; Guo, W.; Xie, Z.; Qu, D.; Liu, D.; Tang, H.; Li, J. A synergistic modification of polypropylene separator toward stable lithium-sulfur battery. *J. Membr. Sci.* **2020**, *597*, No. 117646.
(44) Zhao, H.; Deng, N.; Kang, W.; Wang, G.; Hao, Y.; Zhang, Y.; Cheng, B. The significant effect of octa(aminophenyl)silsesquioxane on the electrospun ion-selective and ultra-strong poly-m-phenyleneisophthalamide separator for enhanced electrochemical performance of lithium-sulfur battery. *Chem. Eng. J.* **2020**, *381*, No. 122715.
(45) Moon, S.; Son, Y.; Kim, S.; Kim, J. The effect of polymer blending and extension conditions on the properties of separator prepared by wet process for Li-ion secondary battery. *Polymer* **2002**, *26*, 45−52.
(46) Qiu, W.; An, C.; Yan, Y.; Xu, J.; Zhang, Z.; Guo, W.; Wang, Z.; Zheng, Z.; Wang, Z.; Deng, Q.; Li, J. Suppressed polysulfide shuttling and improved Li^+ transport in Li−S batteries enabled by NbN Modified PP Separator. *J. Power Sources* **2019**, *423*, 98−105.
(47) Kraft, M. A.; Culver, S. P.; Calderon, M.; Bocher, F.; Krauskopf, T.; Senyshyn, A.; Dietrich, C.; Zevalkink, A.; Janek, J.; Zeier, W. G. Influence of lattice polarizability on the ionic conductivity in the lithium

superionic argyrodites Li_6PS_5X (X = Cl, Br, I). *J. Am. Chem. Soc.* **2017**, *139*, 10909−10918.

(48) Sun, G.; Liu, B.; Niu, H.; Hao, F.; Chen, N.; Zhang, M.; Tian, G.; Qi, S.; Wu, D. In situ welding: Superb strength, good wettability and fire resistance tri-layer separator with shutdown function for high-safety lithium ion battery. *J. Membr. Sci.* **2020**, *595*, No. 117509.

(49) Shin, M.; Song, W. J.; Bin, S. H.; Yoo, S.; Kim, S.; Song, G.; Choi, N. S.; Park, S. Highly stretchable separator membrane for deformable energy-storage devices. *Adv. Energy Mater.* **2018**, *8*, No. 1801025.

(50) Lee, H.; Yanilmaz, M.; Toprakci, O.; Fu, K.; Zhang, X. A review and recent developments in membrane separators for rechargeable lithium-ion batteries. *Energy Environ. Sci.* **2014**, *7*, 3857−3886.

(51) Zhang, Z.; Chen, S.; Yang, J.; Wang, J.; Yao, L.; Yao, X.; Cui, P.; Xu, X. Interface Re-engineering of $Li_{10}GeP_2S_{12}$ electrolyte and lithium anode for all-solid-state lithium batteries with ultralong cycle life. *ACS Appl. Mater. Interfaces* **2018**, *10*, 2556−2565.

(52) Din, M. M. U.; Sahu, B. K.; Das, A.; Murugan, R. Enhanced electrochemical performance of lithium−sulphur battery by negating polysulphide shuttling and interfacial resistance through aluminium nanolayer deposition on a polypropylene separator. *Ionics* **2019**, *25*, 1645−1657.

(53) Haridas, A. K.; Jeon, J.; Heo, J.; Liu, Y.; Saroha, R.; Joo, J. H.; Ahn, H. J.; Cho, K. K.; Ahn, J. H. In-situ construction of iron sulfide nanoparticle loaded graphitic carbon capsules from waste biomass for sustainable lithium-ion storage. *ACS Sustainable Chem. Eng.* **2019**, *7*, 6870−6879.

(54) Fu, W.; Xu, R.; Zhang, X.; Tian, Z.; Huang, H.; Xie, J.; Lei, C. Enhanced wettability and electrochemical performance of separators for lithium-ion batteries by coating core-shell structured silica-poly(cyclotriphosphazene-co-4,4′-sulfonyldiphenol) particles. *J. Power Sources* **2019**, *436*, No. 226839.

(55) Flanagan, M.; Hausman, R.; Digman, B.; Escobar, I. C.; Coleman, M.; Chung, T. S. Surface functionalization of polybenzimidazole membranes to increase hydrophilicity and charge. *ACS Symp. Ser.* **2011**, *1078*, 303−321.

(56) Djian, D.; Alloin, F.; Martinet, S.; Lignier, H.; Sanchez, J. Y. Lithium-ion batteries with high charge rate capacity: Influence of the porous separator. *J. Power Sources* **2007**, *172*, 416−421.

https://doi.org/10.1021/acsomega.2c05472
ACS Omega 2022, 7, 47784−47795